Modeling Dynamics and Stability of 5-axis Milling Processes

E. Ozturk, E. Ozlu,E. Budak*
Sabanci University, Faculty of Engineering and Natural Sciences, Orhanli, Tuzla
34956, Istanbul, Turkey
*ebudak@sabanciuniv.edu

Abstract
5-axis milling is an important machining process for several industries such as aerospace, automotive and die/mold. It is mainly used in machining of sculptured surfaces where surface quality is of extreme importance. Being one of the most important problems in machining, chatter vibrations must be avoided in manufacturing of these components as they result in high cutting forces, poor surface finish and unacceptable part quality. Chatter free cutting conditions for required quality with higher productivity can be determined by using stability models. Up to now, dynamic milling and stability models have been developed for 3-axis milling operations; however the stability of 5-axis processes has never been modeled. In this paper, a stability model for 5-axis milling operations is proposed. The model can consider the 3D dynamics of the 5-axis milling process including effects of all important process parameters including lead and tilt angles. Due to the complex geometry and mechanics of the process, the resulting analytical equations are solved numerically in order to generate the stability diagrams.

1 INTRODUCTION

The 5-axis milling is a heavily used process in manufacturing of complex shaped parts. During the process planning stage, the process planner is faced with several limitations such as high cutting forces, tool deflections and chatter vibrations while selecting proper cutting conditions for higher productivity. Prediction of cutting forces in 5-axis milling was investigated by several researchers [1]-[6]. Ozturk and Budak [6] also predicted tool deflections using the calculated cutting forces in 5-axis ball end milling processes. These studies are helpful for process planner to avoid high cutting forces and unacceptable tool deflections. However, chatter vibrations in 5-axis ball end milling have not been investigated in the past. For that reason, stability limits for chatter free 5-axis ball end milling cannot be predicted before machining. Therefore, a stability model for 5-axis ball end milling processes is required.

The chatter stability of cylindrical end mills was investigated by Minis et al. [7] and Budak and Altintas [8]. Minis et al. [7] solved two-dimensional dynamic milling problem iteratively, using Nyquist stability criterion to determine the stability limits. Budak and Altintas [8] determined the chatter stability directly without any iteration by approximating the time varying coefficients by their Fourier series components. They showed that two-dimensional chatter stability can be predicted analytically as accurately as in time domain simulations. The analytical method was later extended to the prediction of stability limits for ball end milling by Altintas et al. [9]. In this study, the chip thickness variation in both radial and axial directions were considered, and the variation of the cutting force coefficients for each point on the cutting edge were taken into account by transforming shear stress, shear angle and friction angle using the *mechanics of milling method* [10]. The stability limits were determined by solution of a quadratic equation since the dynamics in two dimensions were considered. Later, Altintas [11] extended this model by considering the dynamics in the axial direction. This paper extends the three dimensional chatter stability model to 5-axis ball end milling by adding the effect of lead and tilt angles on the process. The dynamic chip thickness for 5-axis milling is formulated. Depending on the machine tool's kinematics configuration, the feed direction of the tool may change in 5-axis milling due to the lead and tilt angles. Thus, the measured transfer functions need to be oriented accordingly. The effect of this orientation on the stability limits is presented together with effect of lead and tilt angles.

In the next section, 5-axis milling geometry is summarized briefly. Then, the stability limit formulation is given in detail. Finally, the model's

stability limit diagram predictions are demonstrated for different cases.

2 5-AXIS MILLING GEOMETRY

In this section, the geometry of ball-end mill, parameters in 5-axis milling and coordinate systems defining 5-axis process geometry are described.

Ball-end mills are mainly used in 3-axis and 5-axis milling. Since calculation of stability limits requires determination of local cutting edge geometry, the geometry of the ball-end mill is summarized briefly. The geometry of a ball-end mill is shown in Figure 1. A Cartesian tool coordinate system TCS (xyz) is defined at the ball center. The *z*-axis is the axial direction of the cutter. At the tool tip, the local radius *R(z)* is zero, and it increases along the *z*-axis in the ball part whereas it has a constant value of R_o in cylindrical part:

$$\left.\begin{array}{l} R(z) = \sqrt{{R_o}^2 - z^2} \quad for \quad ball \quad part \\ R(z) = R_o \quad\quad for\ cylindrical\ part \end{array}\right\} \tag{1}$$

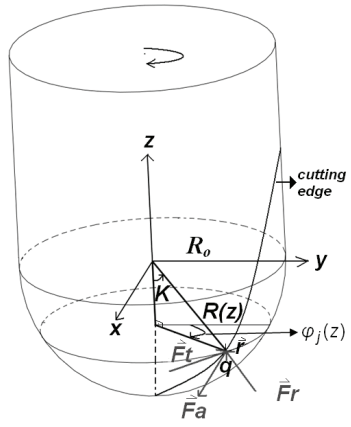

Figure 1: Geometry of ball end mill.

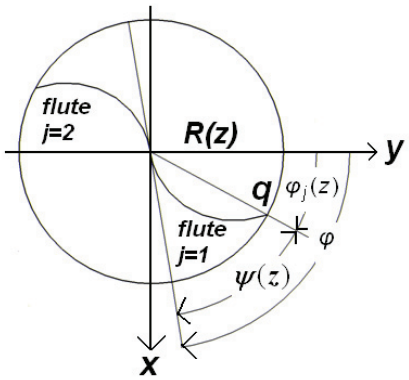

Figure 2: Top view of ball end mill.

A point *q* that is at elevation *z* on a cutting edge has local radius of *R(z),* axial immersion angle of $K = K(z)$, and radial lag angle of $\psi(z)$ (Figure 2). The axial immersion angle *K* is defined as the angle between the tool axis and normal of the cutting edge at point *q*. The axial immersion angle *K* can be calculated as (Figure 1):

$$K = \sin^{-1}\left(\frac{R(z)}{R_o}\right) \tag{2}$$

The radial lag angle $\psi(z)$ is the angle on the *xy* plane between the line which connects the point *q* to the point (0, 0, z), and the cutting edge tangent at the tip of the cutter (Figure 2). Radial lag angle $\psi(z)$ is due to the helix angle, and is calculated using equation 3 [12], where i_o is the helix angle at the meeting point of the ball and the cylinder.

$$\psi(z) = \frac{(R_o + z)}{R_o} \tan i_o \tag{3}$$

Immersion angle $\varphi_j(z)$ shown in Figures 1 and 2 defines the angular orientation of a point on the cutting edge of flute *j*, measured from *+y* direction whereas φ is the immersion angle of the reference tooth at the tool tip. $\varphi_j(z)$ can be expressed as in equation 4:

$$\varphi_j(z) = \varphi + (j-1)\varphi_p - \psi(z) \tag{4}$$

where φ_p is the pitch angle between the preceding flutes.

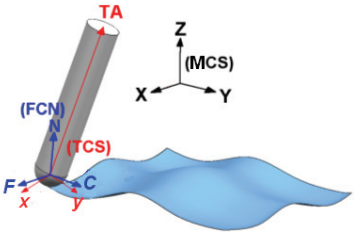

Figure 3: Coordinate systems in 5-axis milling.

In the analysis of 5-axis milling processes, mainly 3 coordinate systems are used: the machine coordinate system (MCS), the process coordinate system (FCN) and the tool coordinate system (TCS) as shown in Figure 3. MCS is a fixed coordinate system attached to the axes of the machine tool. TCS consists of the (*z*) axis which is the tool axis (TA), and the two perpendicular transversal axis (*x*) and (*y*). In FCN, *F* represents the feed direction, *N* stands for the surface normal direction of the workpiece and *C* is the cross-feed axis. The origin of the tool coordinate system (TCS) and the process coordinate system (FCN) is at the ball-center. I

In 5-axis milling, tool orientation is determined by lead and tilt angles which are measured with respect to the surface normal. Lead angle is the

rotation of the tool about the cross-feed axis *C*, and tilt angle is the rotation about the feed axis *F*. Lead and tilt angles are demonstrated in Figure 4.

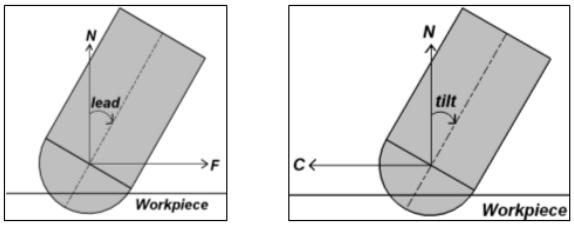

Figure 4: Lead and tilt angles.

Given the process parameters, determining engagement between the tool and workpiece is a crucial step for process modeling. The engagement boundary determination is more complicated in 5-axis milling with respect to 3-axis milling due to effect of lead and tilt angles. In this study, the previously developed engagement model [6] is used to determine the points in cut with the workpiece. In the engagement model, two different cutting types can be considered, namely first cut cases and following cut cases. In the first cut cases, the tool cuts a non-machined cubic solid whereas in the following cut cases it cuts a previously machined surface Figure 5. For the first-cut cases, the radial depth of cut *s* is defined as the distance that the tool penetrates through the workpiece at the ball center level through *C* axis, and the axial depth of cut *a* is the distance between the tool's lowest point and workpiece's upper face in the surface normal direction *N* (Figure 6). For following-cut cases, the radial depth of cut *s* is equal to step over, and the axial depth of cut *a* definition is the same as first-cut cases.

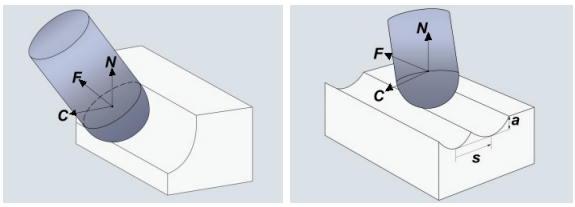

(a) (b)

Figure 5: (a) First and (b) following cut cases.

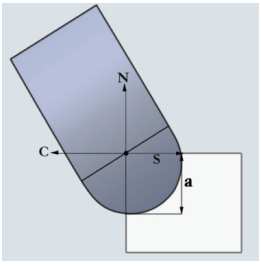

Figure 6: Radial and axial depth definition in first cuts.

3 STABILITY MODEL

The stability model proposed for the 5 axis milling process is derived in this section. Firstly the dynamic chip thickness in 5 axis milling process is modeled. Then, the relationship between the dynamic forces and the chip thickness is derived which is followed by the determination of the stability lobes.

3.1 The dynamic chip thickness

The dynamic chip thickness *h(t)* at a point *q* on the cutting edge consists of two parts, namely static and dynamic parts. The static part *ct* (Figure 7) is determined by the scalar product of the feed vector ***tf*** and unit outward surface normal vector ***u*** at the cutting point *q* where ***f*** is the unit vector in *F* direction, and *t* is the feed per tooth. On the other hand, the dynamic part is calculated by the scalar product of dynamic displacement vector ***d*** and the unit outward surface normal vector ***u*** at the cutting point *q*. Since the static part of the chip thickness *ct* does not contribute to the regeneration mechanism, it can be ignored for the purpose of the stability analysis and the dynamic chip thickness *h(t)* can be written as:

$$h(t) = \mathbf{d} \cdot \mathbf{u} \tag{5}$$

where ***d*** and ***u*** are calculated in the FCN coordinate system. Also, the dynamic displacement vector ***d*** is defined as:

$$\mathbf{d} = \begin{bmatrix} \Delta F_d \\ \Delta C_d \\ \Delta N_d \end{bmatrix} = \begin{bmatrix} F_d(t) - F_d(t-\tau) \\ C_d(t) - C_d(t-\tau) \\ N_d(t) - N_d(t-\tau) \end{bmatrix} \tag{6}$$

where τ is the delay term which is equal to the one tooth passing period in seconds, ΔF_d , ΔC_d and ΔN_d represent the relative displacements difference between the current ($F_d(t)$, $C_d(t)$, $N_d(t)$) and previous relative dynamic displacements ($F_d(t-\tau)$, $C_d(t-\tau)$, $N_d(t-\tau)$) of the tool and the workpiece in *F*, *C* and *N* directions, respectively.

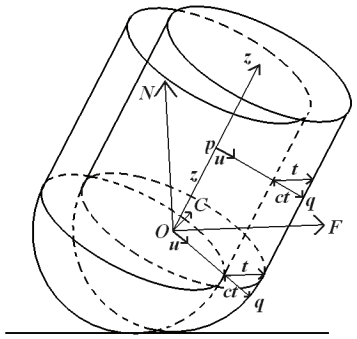

Figure 7: Static part of the chip thickness.

Unit outward surface normal vector $\boldsymbol{u}$ at a point q is calculated in a different way for the ball and the cylinder parts (see Figure 7). For the ball part, the surface normal vector $\boldsymbol{u}$ on the cutting edge can be calculated as:

$$\boldsymbol{u} = \frac{\boldsymbol{Oq}}{|\boldsymbol{Oq}|} = \frac{F\boldsymbol{f} + C\boldsymbol{c} + N\boldsymbol{n}}{R_o} \tag{7}$$

where $\boldsymbol{c}$, $\boldsymbol{n}$ are the unit vectors in C and N axis, respectively. Besides, in the cylindrical part, the unit surface outward normal vector at a point q that is at elevation z is defined as follows:

$$\boldsymbol{u} = \frac{\boldsymbol{pq}}{|\boldsymbol{pq}|} \tag{8}$$

In the calculation of $\boldsymbol{pq}$ vector, first of all the point p is defined. The point p lies in the center of the ball end mill in x and y axis in the TCS coordinate system; and it is at the same elevation with point q in the z axis as shown in Figure 7. Thus, the TCS coordinates of the point p is (0, 0, z). In order to define the $\boldsymbol{pq}$ vector in the FCN coordinates, the point p is transformed to the FCN system using the transformation matrix $\boldsymbol{T}_{lt}$. $\boldsymbol{T}_{lt}$ depends on lead angle l and tilt angle t_ℓ:

$$\boldsymbol{T}_{lt} = \begin{bmatrix} 1 & 0 & 0 \\ 0 & c(t_\ell) & -s(t_\ell) \\ 0 & s(t_\ell) & c(t_\ell) \end{bmatrix} \begin{bmatrix} c(l) & 0 & s(l) \\ 0 & 1 & 0 \\ -s(l) & 0 & c(l) \end{bmatrix} \tag{9}$$

where $s()$ and $c()$ represent sine and cosine functions, respectively. Defining (F_P, C_p, N_p) as the transformed coordinates of the point p in FCN coordinates. The pq vector is calculated as:

$$\boldsymbol{pq} = (F - F_p)\boldsymbol{f} + (C - C_p)\boldsymbol{c} + (N - N_p)\boldsymbol{n} \tag{10}$$

Now, the dynamic chip thickness which corresponds to the ball end and the cylindrical part of the cutter can be calculated by equations 5-10.

3.2 The dynamic forces and the stability limit

In order to apply the stability formulations for dynamic cutting forces, the ball-end mill is divided into disk elements that have heights of Δz along the axial direction of the tool. The cutting forces in x, y and z directions which is on disk element i can be calculated for immersion angle φ_j for each flute j on the tool as:

$$\begin{bmatrix} F_x{}^i(\varphi_j) \\ F_y{}^i(\varphi_j) \\ F_z{}^i(\varphi_j) \end{bmatrix} = \boldsymbol{T} \begin{bmatrix} K_{rc}(\varphi_j, K) \\ K_{tc}(\varphi_j, K) \\ K_{ac}(\varphi_j, K) \end{bmatrix} h(t) \Delta b \tag{11}$$

where K_{rc}, K_{tc} and K_{ac} are cutting force coefficients that are calculated by the transformation of shear angle, friction angle and shear stress using the *mechanics of milling method* [10] and the chip width Δb is calculated using Δz and axial immersion angle K as follows:

$$\Delta b = \frac{\Delta z}{\sin K} \tag{12}$$

$\boldsymbol{T}$ is the transformation matrix which transforms radial, tangential and axial forces to the forces in x, y and z directions that is determined by the below equation in terms of immersion angle φ_j and axial immersion angle K [12]:

$$\boldsymbol{T} = \begin{bmatrix} -s(K)s(\varphi_j) & -c(\varphi_j) & -c(K)s(\varphi_j) \\ -s(K)c(\varphi_j) & s(\varphi_j) & -c(K)c(\varphi_j) \\ c(K) & 0 & -s(K) \end{bmatrix} \tag{13}$$

The dynamic displacement vector $\boldsymbol{d}$ can also be written in terms of displacements in x, y and z directions ($\Delta x_d, \Delta y_d, \Delta z_d$) using the transformation matrix $\boldsymbol{T}_{lt}$ as follows:

$$\boldsymbol{d} = \boldsymbol{T}_{lt} \begin{bmatrix} \Delta x_d \\ \Delta y_d \\ \Delta z_d \end{bmatrix} \tag{14}$$

After the dynamic chip thickness $h(t)$ and the differential chip width Δb are substituted into equation 11, and defining $\boldsymbol{A}^i(\varphi_j)$ matrix as follows:

$$\boldsymbol{A}^i(\varphi_j) = \frac{1}{\sin K} \boldsymbol{T} \begin{bmatrix} K_{rc}(\varphi_j, K) \\ K_{tc}(\varphi_j, K) \\ K_{ac}(\varphi_j, K) \end{bmatrix} \boldsymbol{u}\boldsymbol{T}_{lt} \tag{15}$$

Equation 11 can be rewritten as:

$$\begin{bmatrix} F_x{}^i(\varphi_j) \\ F_y{}^i(\varphi_j) \\ F_z{}^i(\varphi_j) \end{bmatrix} = \Delta z \mathbf{A}^i(\varphi_j) \begin{bmatrix} \Delta x_d \\ \Delta y_d \\ \Delta z_d \end{bmatrix} \tag{16}$$

Summing the cutting forces contributed by all the teeth on disk element i, total dynamic forces at reference immersion angle φ are found as follows:

$$\begin{bmatrix} F_x{}^i(\varphi) \\ F_y{}^i(\varphi) \\ F_z{}^i(\varphi) \end{bmatrix} = \Delta z \mathbf{B}^i(\varphi) \begin{bmatrix} \Delta x_d \\ \Delta y_d \\ \Delta z_d \end{bmatrix} \tag{17}$$

where $\boldsymbol{B}^i(\varphi)$ is the summation of $\boldsymbol{A}^i(\varphi_j)$ for all *n* teeth:

$$\boldsymbol{B}^i(\varphi) = \sum_1^n \boldsymbol{A}^i(\varphi_j) \tag{18}$$

Since the immersion angle φ changes with time, the above equation can be expressed in time domain as:

$$\begin{bmatrix} F_x{}^i(t) \\ F_y{}^i(t) \\ F_z{}^i(t) \end{bmatrix} = \Delta z \mathbf{B}^i(t) \begin{bmatrix} \Delta x_d \\ \Delta y_d \\ \Delta z_d \end{bmatrix} \tag{19}$$

In equation 19, the average component of the Fourier series expansion of $\boldsymbol{B}^i(t)$, which is represented by $\boldsymbol{B_o}^i$, can be used by eliminating the periodic time varying coefficients. $\boldsymbol{B_o}^i$ is a time invariant but immersion dependent coefficient matrix, and it can be calculated by averaging the $\boldsymbol{B}^i(t)$:

$$\boldsymbol{B_o}^i = \frac{1}{\tau}\int_0^\tau \boldsymbol{B}^i(t)dt = \frac{1}{\varphi_p}\int_o^{\varphi_p} \boldsymbol{B}^i(\varphi)d\varphi \tag{20}$$

Using $\boldsymbol{B_o}^i$, equation 20 reduces to:

$$\begin{bmatrix} F_x{}^i(t) \\ F_y{}^i(t) \\ F_z{}^i(t) \end{bmatrix} = \Delta z \mathbf{B_o}^i \begin{bmatrix} \Delta x_d \\ \Delta y_d \\ \Delta z_d \end{bmatrix} \tag{21}$$

The dynamic displacement vector in TCS can be defined in terms of the transfer function of the structure and cutting forces as:

$$\begin{bmatrix} \Delta x_d \\ \Delta y_d \\ \Delta z_d \end{bmatrix} = (1 - e^{-iw_c\tau})\boldsymbol{G}(i\omega_c) \begin{bmatrix} F_x(t) \\ F_y(t) \\ F_z(t) \end{bmatrix} \tag{22}$$

where ω_c is chatter frequency; $F_x(t)$, $F_y(t)$, $F_z(t)$ are total dynamic cutting forces in TCS coordinate system and $\mathbf{G}(i\omega_c)$ is the transfer function identified at the cutter workpiece contact zone oriented with respect to the TCS coordinate system. The orientation of transfer function is needed because transfer functions are measured in fixed machine coordinate system (MCS). The orientation is performed using a transformation matrix $\boldsymbol{T_G}$ which depends on orientation of FCN with respect to MCS, lead and tilt angles as follows:

$$\boldsymbol{T_G} = \begin{bmatrix} f_X & c_X & n_X \\ f_y & c_Y & n_Y \\ f_Z & c_Z & n_Z \end{bmatrix} \boldsymbol{T_{It}} \tag{23}$$

where f_X, f_Y, f_Z ; c_X, c_Y, c_Z; n_X, n_Y, n_Z are the measure numbers of unit feed vector, unit cross-feed vector and unit surface normal vector in MCS, respectively. The transformation of a transfer function $\boldsymbol{H}(i\omega_c)$ measured in MCS to TCS is done using below equation:

$$\boldsymbol{G}(i\omega_c) = \boldsymbol{T_G}^T \boldsymbol{H}(i\omega_c)\boldsymbol{T_G} \tag{24}$$

where superscript *T* denotes the transpose operation.

Inserting equation 22 into equation 21, the dynamic cutting force system on disk *i* becomes:

$$\begin{bmatrix} F_x{}^i \\ F_y{}^i \\ F_z{}^i \end{bmatrix} e^{i\omega_c t} = \Delta z \boldsymbol{B_o}^i (1 - e^{-i\omega_c\tau})[G(i\omega_c)] \begin{bmatrix} F_x \\ F_y \\ F_z \end{bmatrix} e^{i\omega_c t} \tag{25}$$

Now the dynamic elemental forces can be calculated using Equation 25 for each disk element. However, in order to obtain the stability limit of the system, all the disk elements have to be solved simultaneously. We propose to add the individual dynamic forces acting on each element together. Thus, writing this equation for the other disk elements and summing up the equations side by side results in the following eigenvalue problem:

$$\begin{bmatrix} F_x \\ F_y \\ F_z \end{bmatrix} e^{i\omega_c t} = -\Lambda\left(\sum_{i=1}^m \left[\boldsymbol{B_o}^i(K)\right]\right)[G(i\omega_c)] \begin{bmatrix} F_x \\ F_y \\ F_z \end{bmatrix} e^{i\omega_c t} \tag{26}$$

where *m* is the total number of disk elements and Λ is the eigenvalue . Equation 26 has solution if and only if the following determinant is equal to zero:

$$\det\{\boldsymbol{I} + \Lambda\boldsymbol{\Phi}\} = 0 \tag{27}$$

where $\boldsymbol{\Phi}$ and complex eigenvalue Λ are defined as follows:

$$\begin{aligned} \boldsymbol{\Phi} &= \left[\sum_{i=1}^m \mathbf{B_o}^i(K)\right][G(i\omega_c)] \\ \Lambda &= -\Delta z(1 - e^{-i\omega_c\tau}) = \Lambda_R + i\Lambda_I \end{aligned} \tag{28}$$

Substituting $e^{-iw_c\tau} = \cos w_c\tau - i\sin w_c\tau$ into eigenvalue equation, critical depth at chatter frequency w_c can be written as [8]:

$$\Delta z_{\lim} = -\frac{1}{2}\left[\frac{\Lambda_R(1-\cos\omega_c\tau) + \Lambda_I\sin\omega_c\tau)}{(1-\cos\omega_c\tau)} + i\frac{\Lambda_I(1-\cos\omega_c\tau) - \Lambda_R\sin\omega_c\tau)}{(1-\cos\omega_c\tau)}\right] \tag{29}$$

Since Δz_{lim} is a real number, the imaginary part of equation 29 vanishes and following relation is obtained:

$$\Lambda_I(1-\cos\omega_c\tau)=\Lambda_R\sin\omega_c\tau \quad (30)$$

Defining $\kappa=\frac{\Lambda_I}{\Lambda_R}=\frac{\sin\omega_c\tau}{1-\cos\omega_c\tau}$, the critical depth Δz_{lim} can be found as:

$$\Delta z_{\lim}=-\frac{1}{2}\Lambda_R(1+\kappa^2) \quad (31)$$

3.3 Stability diagrams

In the foregoing analysis, the basic stability limit prediction for 5 axis milling process is derived. However, it should be noted that there are two unknowns in the formulation, the total number of disk elements m and the height of the disks Δz. In order to solve the dynamic system's stability with these two unknowns an iterative solution procedure is proposed as follows.

The solution begins by selecting a Δz value. Then, the stability limit Δz_{lim} is calculated starting from the first element and incrementing m one by one. For each iteration, it is checked whether the calculated stability limit Δz_{lim} is smaller than Δz. If it is so, limiting depth of cut z_{lim} is obtained as $m\Delta z$ otherwise the iteration continues by considering the next disk element. Since the calculated limiting depth of cut z_{lim} is along the tool axis direction, it is transformed to the surface normal direction to find the limiting depth of cut a_{lim}. It should be mentioned here that selecting smaller Δz values increases the accuracy of the solution. Once the stable depth of cut is obtained by sweeping the chatter frequency around the most flexible modes of the dynamic system, the corresponding spindle speed can be calculated as proposed in [8]. The following equation defines the relation between the chatter frequency w_c and tooth passing period τ:

$$w_c\tau=\varepsilon+2k\pi \quad (32)$$

where ε is the phase shift between the present and the previous vibration waves and k is the integer number of full vibration waves marked on the cut. Phase shift depends on phase angle $\varphi_{ph}=\tan^{-1}\kappa$, and is determined by:

$$\varepsilon=\pi-2\varphi_{ph} \quad (33)$$

The corresponding spindle speed n_s can be calculated after tooth passing period τ is calculated:

$$\tau=\frac{1}{\omega_c}(\varepsilon+2k\pi)\rightarrow n_s=\frac{60}{nT} \quad (34)$$

Finally the stability lobes can be obtained by plotting the corresponding stable depth of cut and spindle speed values.

4 SIMULATIONS

In this section, the proposed stability model's predictions are presented for different example cases. Firstly the proposed model is compared with CutPro®[13] software for a special case of 3-axis ball end milling operations. Then the effect of using the oriented transfer function is discussed. Finally the effect of the lead and tilt angles on the stability limit is presented.

Following are the common parameters that are used in the simulations. The cutting tool used in the simulations is a 2 flute 8mm diameter ball end mill with 8° rake and 30° helix angle. Dynamics of the workpiece is neglected as it is highly rigid with respect to the cutting tool. Transfer function of the tool is measured in MCS using hammer test. The dynamics in the Z direction H_{ZZ} is neglected since the tool is very stiff in Z direction with respect to X and Y directions. Moreover, the cross terms in the transfer function matrix are ignored.

A special case, where lead and tilt angles are zero, is simulated both with the proposed stability model and CutPro® software. The example case is a 3-axis ball-end milling slotting operation. Workpiece material is selected as Ti6Al4V and cutting coefficients are determined by *mechanics of milling method*. Feed per tooth is 0.05 mm/tooth. The comparison of the model's and Cutpro®'s predictions for stability lobes are presented in Figure 8.

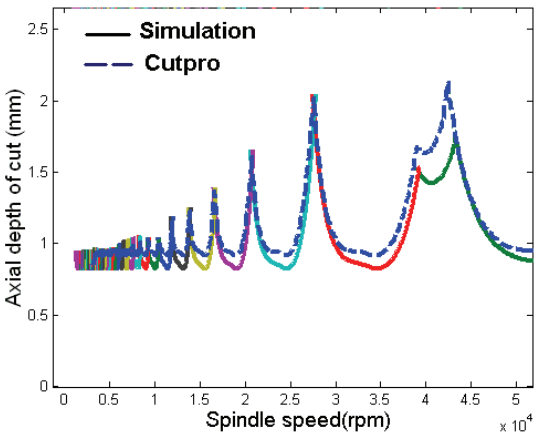

Figure 8: Comparison of the results of the model and Cutpro®

Comparing the model's prediction with Cutpro®, it's seen that there is an acceptable difference between the predictions which may be due to different treatment of the cutting force coefficients.

4.1 The effect of the oriented transfer function on the stability limit

Being the major difference from the conventional milling operations, the lead and tilt angles in five axis milling operations affect the mechanics of the process by changing the orientation of the tool according to the workpiece surface. Furthermore, depending on the kinematic configuration of the machine tool, they may change the directions of feed, cross-feed and surface normal directions with respect to fixed machine coordinate system MCS. If transfer functions of the tool and/or workpiece are direction dependent, then directions of feed, cross-feed and surface normal direction becomes important in terms of stability. In these cases, the measured transfer functions need to be oriented accordingly.

The five axis CNC machine in our lab has two rotary degrees of freedom on the table. Since lead and tilt angles are applied by rotating the table, the feed direction given with respect to the workpiece on the table becomes dependent on lead and tilt angles according to fixed coordinate system MCS. Hence, for such machine tools lead and tilt angles change the oriented transfer function as well as the mechanics of the process. However, if the rotary axes are on the spindle side, then the lead and tilt angles do not change the direction of feed, and thus transfer functions. The second example simulation shows the effect of orientation of the measured transfer function on stability. In the first case, the machine tool has two rotary degree of freedoms on the table and in the second case a machine tool where all rotary degree of freedoms are on the spindle is used. For both cases the same process which is a following cut operation is simulated. Lead and tilt angles are both 15 deg, radial depth of cut is 2 mm and feed per tooth is 0.05 mm. The workpiece material is 1050 steel. Figure 9 shows the axial stability limit diagram prediction of the model when first type of machine is used. Since feed, cross-feed and surface normal directions change with the application of lead and tilt angles, the oriented transfer function is used in this case. For the second machine tool type, the measured transfer function is directly used in the stability formulation. The stability limit diagram prediction for this case is presented in Figure 10. It's seen that for these two sample cases, the orientation of the transfer function, i.e. the kinematic configuration of the machine tool, has a considerable effect on the stability limits. Absolute stability limit prediction is 6 mm for the first case whereas it's 1 mm in the second case.

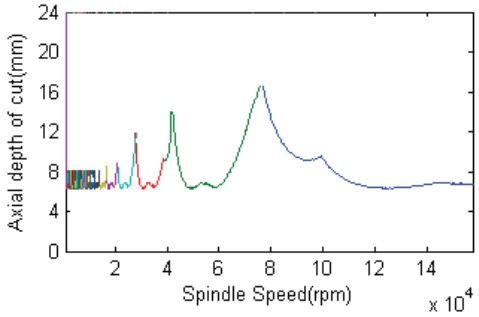

Figure 9: Stability limit diagram when oriented transfer function is used.

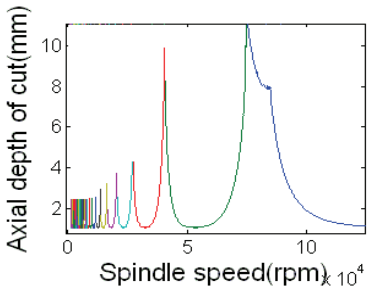

Figure 10: Stability limit diagram when no orientation is used.

4.2 The effect of the lead and tilt angles on the stability limit

In order to observe the effect of the tilt and lead angles together with the oriented transfer function effect, simulations are conducted for the case in Section 4.1 by varying the tilt and the lead angles. The results when the oriented transfer function is used are shown in Figure 11. On the contrary, in order to exclude the effect of the orientation, the same process is simulated where the orientation of transfer function is not considered. For this case, the effect of the lead and tilt angles on the absolute stability limit is presented in Figure 12. In both of the cases absolute stability limit prediction is same for *lead*=0 deg and *tilt*=0 deg case because no orientation is needed in this case. Another important conclusion from the results is the high difference between the absolute stability limit for the two cases. With the integration of the orientated transfer function in the prediction, the stability limit is found to be much higher than the predictions without oriented transfer function. These results can be used to determine optimal lead and tilt angles for increased stability.

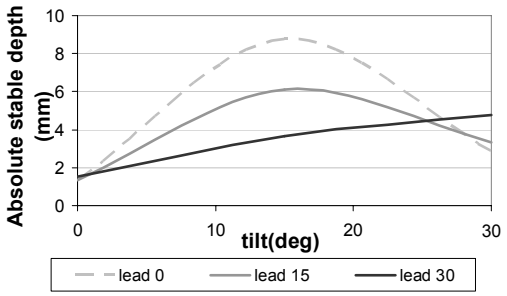

Figure 11: Effect of lead and tilt angles when oriented transfer function is used.

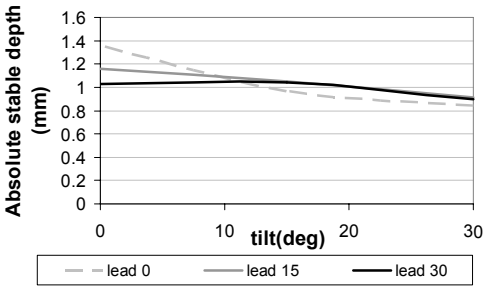

Figure 12: Effect of lead and tilt angles when orientation is not used.

5 CONCLUSION

In this paper, a stability limit model for 5-axis milling process is presented where the dynamic chip thickness is formulated in 5-axis ball end milling together with the dynamic cutting forces. The ball end mill is divided into disk elements and the stability limit of the dynamic system is solved iteratively. For 3-axis ball end milling slotting case the predictions of the stability model is compared with CutPro® predictions and good agreement is observed. In 5-axis milling, for two different machine tool configurations, stability limit diagrams are predicted and the effect of using the oriented transfer function is shown. Finally, effects of lead and tilt angles on the stability limit are demonstrated. The experimental verification of the presented stability model for 5-axis ball end milling is currently under progress.

6 ACKNOWLEDGEMENTS

The authors acknowledge Scientific and Technical Research Council of Turkey (TUBITAK) for its support in this research.

7 REFERENCES

[1] Clayton, P. A., El-Wardany, T., Elbestawi, M. A., Viens D., 2000, A Mechanistic Force Model of the 5-axis Milling Process, Proceedings of the ASME Manufacturing Engineering Division, 11, 979-987.

[2] Zhu, R., Kapoor, S. G., DeVor, R. E., 2001, Mechanistic Modeling of the Ball End Milling Process for Multi-axis Machining of Free-form Surfaces, Journal of Manufacturing Science and Engineering, 123, 369-379.

[3] Fussell, B.K., Jerard, R. B., Hemmet, J. G., 2003, Modeling of Cutting Geometry and Forces for 5-axis Sculptured Surface Machining. Computer Aided Design, 35, 333-346.

[4] Larue, A., Altintas, Y., 2005, Simulation of Flank Milling Processes, International Journal of Machine Tools and Manufacture, 45, 549-559.

[5] Lopez de Lacalle, L. N., Lamikiz, A., Sanchez, J. A., Salgado, M. A., 2007, "Toolpath Selection Based on the Minimum Deflection Cutting Forces in the Programming of Complex Surfaces Milling" International Journal of Machine Tools and Manufacture, 47(2), 388-400.

[6] Ozturk, E. and Budak, E., "Modeling of 5-Axis Forces", Proceedings of the 8th International Workshop on Modeling of Machining Operations, pp. 319-326, Chemnitz, Germany, May 10-11, 2005.

[7] Minis, I., Yanushevsky, T, Tembo, R. and Hocken, R., Analysis of Linear and Nonlinear Chatter in Milling, Annals of the CIRP, Vol.39, pp.459-462.

[8] Budak, E., Altintas, Y., 1998, Analytical Prediction of Chatter Stability in Milling. Part I: General Formulation, Part II: Application of the General Formulation to Common Milling Systems, Transactions of ASME, Vol. 120, pp 22-36.

[9] Altintas, Y., Shamoto, E., Lee, P., Budak, E., 1999, Analytical Prediction of Stability Lobes in Ball End Milling, Transactions of ASME, Vol. 121, pp 586-592.

[10] Budak, E., Altintas, Y., Armarego, E. J. A., 1996, Prediction of Milling Force Coefficients from Orthogonal Cutting Data, Journal of Manufacturing Science and Engineering., 118, 216-224.

[11] Altintas, Y., 2001, Analytical Prediction of Three Dimensional Chatter Stability in Milling, JSME International Journal, Series C, Vol. 44, No. 3,pp.717-72.

[12] Lee, P., Altintas, Y., 1996, Prediction of Ball End Milling Forces from Orthogonal Cutting Data, International Journal of Machine Tools and Manufacture, 36, 1059-1072.

[13] http://www.malinc.com (CutPro® website)